# Triaxiality in $^{105}$Mo and $^{107}$Mo from the low to intermediate spin region

J. A. Pinston,[1] W. Urban,[2] Ch. Droste,[2] T. Rząca-Urban,[2] J. Genevey,[1] G. Simpson,[1] J. L. Durell,[3] A. G. Smith,[3] B. J. Varley,[3] and I. Ahmad[4]

[1]*Laboratoire de Physique Subatomique et de Cosmologie, IN2P3-CNRS/Université Joseph Fourier, F-38026 Grenoble Cedex, France*

[2]*Faculty of Physics, Warsaw University, ul. Hoża 69, 00-681 Warsaw, Poland*

[3]*Department of Physics and Astronomy, University of Manchester, Manchester M13 9PL, United Kingdom*

[4]*Argonne National Laboratory, Argonne, Illinois 60439, USA*

(Received 3 July 2006; revised manuscript received 8 September 2006; published 6 December 2006)

The nuclear structure of the odd $^{105}$Mo and $^{107}$Mo isotopes was reinvestigated in the present work. The excited levels of $^{105}$Mo were studied by observing prompt $\gamma$ rays emitted after the spontaneous fission of $^{248}$Cm with the EUROGAM2 multidetector array. The already well-studied level structure of $^{107}$Mo was also completed by a search for microsecond isomers. For this purpose, this nucleus was produced by the thermal-neutron-induced fission reaction at the ILL reactor, in Grenoble. We have shown that the experimental level energies and the $\gamma$-decay patterns are well reproduced by simple particle-rotor calculations, assuming that these nuclei have an asymmetric shape. The shapes of the odd and even Mo are compared in the neutron range $N = 62$–$66$.

DOI: 10.1103/PhysRevC.74.064304 PACS number(s): 21.10.Tg, 23.20.Lv, 25.85.Ec, 27.60.+j

## I. INTRODUCTION

A large variety of shapes may be observed in Sr and Zr nuclei of the $A = 100$ region when the neutron number increases from 58 to 64. The lighter isotopes up to $N = 58$ are rather spherical. It is also well established [1] that three shapes coexist in the transitional odd-A, $N = 59$ Sr and Zr nuclei: the ground state and low-lying states are nearly spherical, whereas deformed bands with intermediate deformation [$\beta_2 = 0.32(2)$, $\epsilon_2 = 0.27$] are present at about 600 keV and the maximum deformation [$\beta_2 = 0.40(2)$, $\epsilon_2 = 0.33$] of the region is reached for the 9/2[404] band at about 1 MeV of excitation. These three different shapes are also present in $^{101}$Zr. For $N > 59$, strongly deformed axially symmetric bands are observed in Sr and Zr nuclei, although shape coexistence phenomena are still present in even-even nuclei with $N = 60$. Moreover, it has been shown in Ref. [1] that the Nilsson orbitals originating from the $\nu(h_{11/2})$ and $\nu(g_{9/2})$ unique-parity states play a dominant role in explaining the origin of the deformation and the shape coexistence phenomena of this region. In this simple picture the maximum deformation is obtained when four core particles occupy the 1/2[550] and 3/2[541] down-slopping orbitals, while there is no longer a pair in the 9/2[404] upslopping orbital.

In the even-even $^{104-108}$Mo a new situation occurs [2–4]. These nuclei are strongly deformed ($\beta_2 \approx 0.38$, see Sec. IV below), but at the same time, the levels of the $K^\pi = 2^+$ $\gamma$ band go down in energy with the increase of the neutron number, suggesting that the triaxial degree of freedom plays an important role in these isotopes. However, the nature of the triaxiality in these even-Mo isotopes is not well understood. The calculations of Skalski *et al.* [5] predict ground-state triaxial minima, $\gamma = 19^\circ$–$21^\circ$, for these nuclei. In contrast, the article of Smith *et al.* [2] suggests that the triaxiality is likely to be dynamic in nature, with a deformation $\gamma \approx 0^\circ$ at low spins and a rotation-induced change in triaxiality at moderate spins. The last effect is supported by the experimental observation of a decrease of the quadrupole moment at spins $I \approx 10$–$12$. At higher spins, Hua *et al.* [4] have measured the crossing frequency of the $g$ and $S$ band in $^{102-108}$Mo. From a comparison with the cranked shell model, they have deduced a quadrupole deformation $\beta_2 = 0.33$ and a triaxial deformation $\gamma = 19^\circ$, for $^{104}$Mo only. The deformations for the other Mo were not reported, very likely because the crossing frequency values change considerably between $^{102}$Mo and $^{108}$Mo. It is worth noting that the deformation deduced from the crossing frequency could differ from that of the low-spin region, due to the mixing between the $g$ and $\nu(h_{11/2})^2$ band. This effect is observed in the calculculations of Skalski *et al.* and is especially strong in $^{106}$Mo and $^{108}$Mo.

The experimental study of the triaxiality is much less advanced for the odd Mo nuclei, where mainly the $5/2^-$ band, originating from the $\nu h_{11/2}$ spherical orbital, was investigated in $^{103}$Mo and $^{105}$Mo. Recently, triaxial deformation values of $\gamma = 20^\circ$ [4] and $19^\circ$ [6] were deduced from the signature splitting of the $5/2^-$ band in $^{103}$Mo and $\gamma = 15^\circ$ for $^{105}$Mo [6]. It is worth noting that in $^{103}$Mo the authors of Ref. [6] have found a different triaxial deformation for the $5/2^-$ band ($\gamma = 20^\circ$) and $3/2^+$ band ($\gamma = 8^\circ$). No information on triaxiality is reported for $^{107}$Mo.

Better understanding of the nature of the nonaxial deformation in odd-$A$ Mo isotopes requires the study of the structure of several bands in the same nucleus. For this reason, the $^{105}$Mo and $^{107}$Mo nuclei have been revisited experimentally in the present work and the structure of these nuclei was analyzed in the framework of the particle-rotor coupling model, in the low-to-intermediate spin region. The $^{105}$Mo nucleus was populated in spontaneous fission of $^{248}$Cm and prompt $\gamma$ rays following fission were measured using the EUROGAM2 array. Four well-developed bands were observed in $^{105}$Mo. In $^{107}$Mo, three well-developed bands were previously reported from $\gamma$-ray measurements of the spontaneous fission of $^{248}$Cm [7]. To complete the level scheme, this nucleus has been produced through thermal-neutron-induced fission reaction of a $^{241}$Pu target, at the ILL reactor in Grenoble. In this case, the LOHENGRIN mass spectrometer was used

 

to look for $\mu$s isomers and to measure delayed $\gamma$ rays and conversion electrons deexciting these isomers. A new isomer with a half-life of 420 ns was observed in this work. It has been tentatively assigned as a $1/2^+$ state deexciting by an $E2$ transition to the $5/2^+$ ground state. This wealth of information in $^{105}$Mo and $^{107}$Mo, which is unique in the neutron-rich odd Mo isotopes, makes a comparison in the frame of the rotational model meaningful.

In the following sections, we present detailed experimental results and our analysis for the nuclear structure of $^{105}$Mo and $^{107}$Mo nuclei. Section II contains a description of the experimental methods and presents the results of our new measurement of $^{105}$Mo and $^{107}$Mo. In Sec. III, the level energies and the $\gamma$-decay patterns of these two nuclei are calculated using a particle-rotor model of a single quasiparticle coupled to an asymmetric core. In Sec. IV, the deformations of the odd and even-even Mo are compared. Section V summarizes our results.

## II. EXPERIMENTAL PROCEDURES AND THE RESULTS

### A. Prompt $\gamma$-ray experiment

The nucleus $^{105}$Mo was previously studied in $\beta^-$ decay of $^{105}$Nb [8–10], in spontaneous fission of $^{248}$Cm [11] and $^{252}$Cf [12] and in $^{238}$U($\alpha$, $f$) reaction [4]. In these studies four different configurations were proposed in $^{105}$Mo but the only well-developed band was observed to feed the ground state [4,11,12].

In the present work we have studied the $^{105}$Mo nucleus, populated in spontaneous fission of $^{248}$Cm. Prompt $\gamma$ rays following the fission process were measured using the EUROGAM2 array with four additional low-energy photon (LEP) detectors (for more details on the experiment and data analysis techniques see [13–15]).

The ground state of $^{105}$Mo has a spin and parity $I^\pi = 5/2^-$ [9,11] and the rotational band built on this level is now known up to spin $39/2^-$ [4]. In our data this band is well seen and corresponds to the band 1 of the level scheme of Fig. 1. The spectrum doubly gated on the 418- and 557-keV lines in this band, shown in Fig. 2(a), illustrates the quality of our coincidence data. The spectrum fully agrees with Refs. [4,12]. We note that the 694- and 826-keV lines are broadened due to the Doppler effect, observed in our data above spin $I = 8$ for rotational bands [2]. A large signature splitting is observed in this band and is compared in Fig. 3 with the staggering evidenced for the $7/2^-$ band in $^{107}$Mo and reported in our recent work [7].

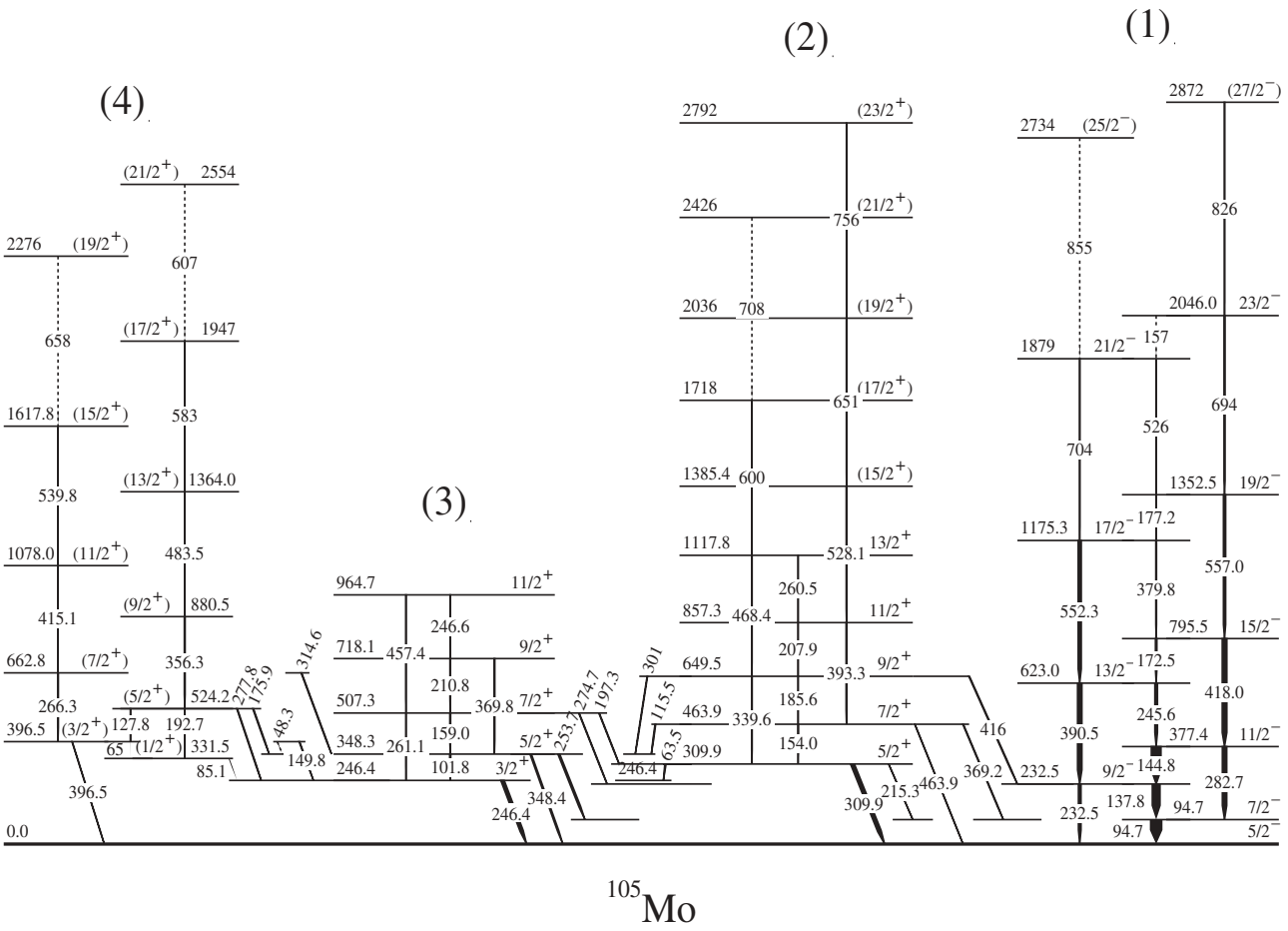


FIG. 1. Partial level scheme of $^{105}$Mo as obtained in this work. Arrow thickness is proportional to the relative $\gamma$ intensities of transition. Uncertainties on $\gamma$ energies are from 0.1 keV for strong lines and up to 0.5 keV for weak lines.

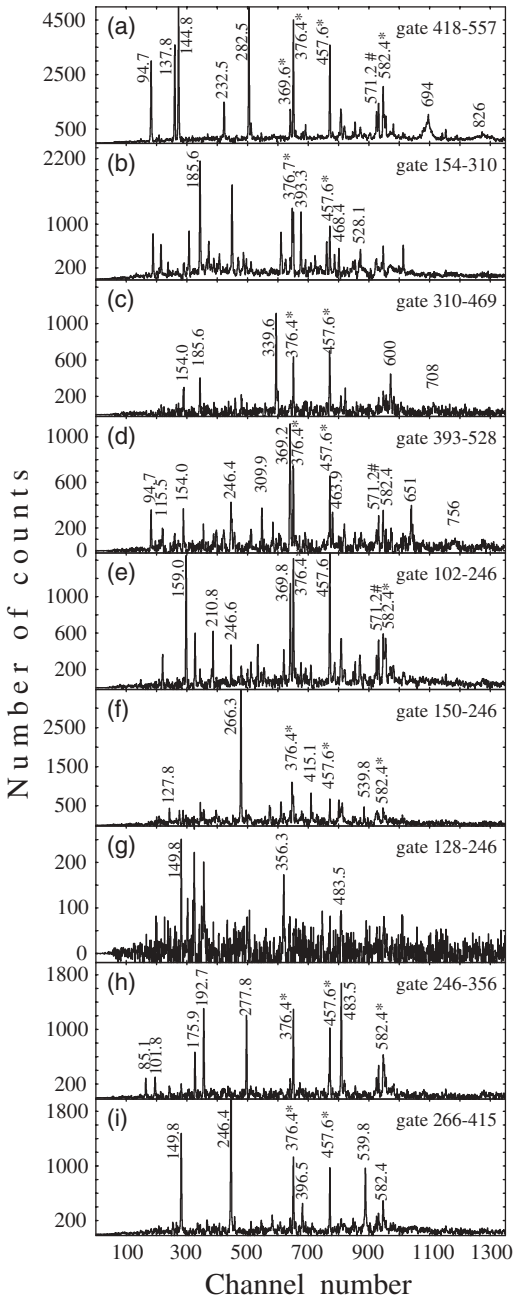


FIG. 2. Coincidence spectra gated on $\gamma$ lines in $^{105}$Mo. Energies of lines are given in keV. The asterisk denotes lines in $^{140}$Xe. Unlabeled lines are from contaminating nuclei.

A double gate set on the 309.9- and 154.0-keV lines, reported in Ref. [10] as transitions in $^{105}$Mo, shown in Fig. 2(b), reveals a rich spectrum, in which lines of the complementary Xe isotopes are seen as well as many unknown lines, among them 185.6-, 393.3-, 468.4-, and 528.1-keV lines. In Fig. 2(c) we show a spectrum doubly gated on the 309.9-keV line and the new 468.4-keV line. One observes here the 154.0- and 185.6-keV lines seen in Fig. 2(b) as well as new lines at 339.6, 600, and 708 keV. Finally, in Fig. 2(d) we show a spectrum doubly gated on the new 393.3- and 528.1-keV lines. We note broad shapes of the 651- and 756-keV lines in Fig. 2(d) and

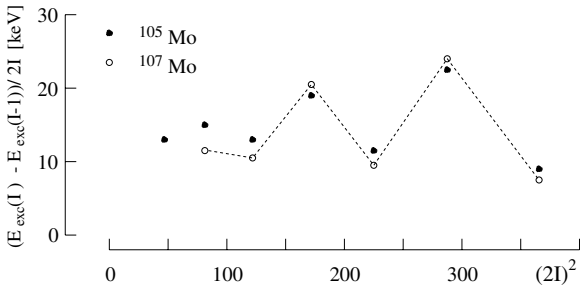


FIG. 3. Staggering in the negative-parity bands of $^{105}$Mo and $^{107}$Mo [5]. The dashed line is drawn to guide the eye.

the 708-keV line in Fig. 2(c). These spectra and further gates allowed the construction of the band 2 on top of the 309.9-keV level, as shown in the level scheme of Fig. 1. Spin and parity $5/2^+$ for the 309.9-keV level were proposed in Ref. [10], from $\beta$-decay experiment and the first excited state of the band at 463.9 keV is also reported by these authors. In the present work, this band was extended up to spin $(23/2^+)$.

The levels of band 3 at $246(3/2^+)$, $348(5/2^+)$, and 507 keV $(7/2^+)$ were previously observed in a $\beta$-decay experiment [10]. This result is confirmed in the present experiment. In the spectrum doubly gated on the 246.4- and 101.8-keV lines [see Fig. 2(e)], one sees lines of the complementary Xe isotopes and new lines at 159.0, 210.8, 246.6 (self-gating), 369.8, and 457 keV (the 457 keV line belongs also to $^{140}$Xe, explaining its high intensity). Further gating allowed the construction of a regular band built on the 246.4 keV level as shown in Fig. 1. It consists of five levels. We note that the population of the highest band member at 964.7 keV is rather strong, suggesting a continuation of this band. Unfortunately, due to the complex nature of many lines in this band (transitions of similar energy being present in other nuclei), it was not possible to establish without doubts higher levels in this band.

In the spectrum doubly gated on the 246.4- and 149.8-keV lines and shown in Fig. 2(f), there are the 266.3-, 415.1-, and 539.8-keV lines already reported in Ref. [4]. In the 127.8- to 246.4-keV double gate, shown in Fig. 2(g), one can see a new line at 356.3 keV. The double gate, 246.4–356.3 keV, shown in Fig. 2(h), reveals the 175.9-, 192.7-, and 277.8-keV lines, which were reported in Ref. [8] as deexciting the 524.2-keV level. Further gating allowed the construction of band 4, shown in Fig. 1. The band head, located at 331.5 keV, was suggested in Ref. [10] to have a spin and parity $1/2^+$. We adopt this assignment, which is further discussed in the next section. The cascade built on the 331.5-keV level, consisting of the 192.7-, 356.3-, 583-, and 607-keV transitions, and the cascade on top of the 396.5-keV level, consisting of the 266.3-, 415.1-, 539.8-, and 658-keV transitions, communicate with each other at the low-energy part via 65- and 127.8-keV transitions (the 65- and 48.3-keV transitions, shown in Fig. 1, are not directly observed but their presence in the level scheme is indicated by the observed coincidence relations. The 48-keV transition was reported also in Ref. [8]). We therefore assign both cascades to the $1/2^+$ band. We note that the $I = 1/2^+$ spin assignment to the 331.5-keV level is consistent with the

nonobservation of any decay of this level to the $I = 5/2^-$ ground state. In contrast, we see in our data a 396.5-keV transition feeding the ground state, as illustrated in Fig. 2(i), showing $\gamma$ spectrum doubly gated on the 266.3- and 415.2-keV lines. This observation is consistent with a spin and parity assignment $3/2^+$ for the 396.5-keV level. We note that despite the low spin of the 331.5-keV band head, the band on top of it is close to the yrast line, when compared to the other two bands of positive parity. Therefore its population in fission is nonnegligible.

Energies and relative intensities of $\gamma$ transitions in $^{105}$Mo, as observed in our measurement, are shown in Table I.

### B. The LOHENGRIN experiment

Microsecond isomers were investigated in the mass chain $A = 107$ at the ILL reactor in Grenoble. These nuclei were produced by thermal-neutron-induced fission, using a thin target of about 400 $\mu$g/cm$^2$ of $^{241}$Pu. The Lohengrin mass spectrometer was used to separate the fission fragments (FFs) recoiling from the target, according to their mass to ionic charge ratios ($A/q$). Two different setups were used. In the first one the FFs were detected in a gas detector of 13 cm length and subsequently stopped in a 12-$\mu$m-thin Mylar foil. Behind the foil, two cooled adjacent Si(Li) detectors covering an area $2 \times 6$ cm$^2$ were placed to detect the conversion electrons and x rays, whereas the $\gamma$ rays were detected by two 60% Ge detectors placed perpendicular to the beam. This setup allows conversion electrons to be detected down to low energy (15 keV) and allows $\gamma$-electron coincidences to be obtained. Details on this experimental setup can be found in Refs. [16,17].

In the second setup, the FFs were detected in an ionization chamber filled with isobutane at a pressure of 47 mb. This ionization chamber has good nuclear charge ($Z$) identification. It consists of two regions of gas $\Delta E1$ and $\Delta E2$, separated by a grid, which are 9 cm and 6 cm long, respectively. This system is able to identify the nuclear charge in the $Z \approx 40$ region, with a resolution (FWHM) of about two units. The $\gamma$ rays deexciting the isomeric states were detected by two Clover detectors placed perpendicular to the ion beam in a very close geometry, thanks to the small thickness (6 cm) of the ionization chamber. The total efficiency for the $\gamma$ detection was 20 and 4% for photons of 100 keV and 1 MeV, respectively. More details on this experimental setup can be found in Ref. [18].

With the two setups we have observed a new $\mu$s isomer deexciting by a single $\gamma$ ray of 65.4 keV. Based on the time spectrum of the isomer, shown in Fig. 4, a half-life value of 420(30) ns was determined. The assignment of the isomer to the atomic number $Z = 42$ was confirmed by the measurement of the energy loss of the ions in the first stage of the ionization chamber. The energy loss was measured in coincidence with the $\gamma$ ray deexciting the 65.4-keV isomer. This energy can be compared with the energy loss of the whole distribution of the different isotopes of mass $A = 107$, which was also measured. The comparison shown in Fig. 5 allows an unambiguous atomic charge identification.

The spectrum obtained from the Si detector is shown in Fig. 6. Narrow peaks corresponding to x and $\gamma$ rays and broad

TABLE I. Gamma transitions in $^{105}$Mo as observed in the radiation following spontaneous fission of $^{248}$Cm. In column 1(4) and 2(5) the experimental $\gamma$-ray energy and initial-level energy are reported, respectively. In column 3(6) $\gamma$-ray intensities are shown.

| $E_\gamma$ (keV) | $E_{exc}$ (keV) | $I_\gamma$ relative | $E_\gamma$ (keV) | $E_{exc}$ (keV) | $I_\gamma$ relative |
|---|---|---|---|---|---|
| 63.5 | 309.9 | 9 (2) | 314.6 | 662.8 | 2.1(3) |
| 85.1 | 331.5 | 7 (1) | 339.6 | 649.5 | 5 (1) |
| 94.7 | 94.7 | 100 (3) | 348.4 | 348.3 | 11 (1) |
| 101.8 | 348.3 | 9 (1) | 356.3 | 880.5 | 6.9(7) |
| 115.5 | 463.9 | 6 (1) | 369.2 | 463.9 | 5.3(5) |
| 127.8 | 524.2 | 2.3(4) | 369.8 | 507.3 | 5.8(5) |
| 137.8 | 232.5 | 74 (3) | 379.8 | 1175.3 | 5.5(5) |
| 144.8 | 377.4 | 77 (3) | 390.5 | 623.0 | 35 (2) |
| 149.8 | 396.5 | 4.7(8) | 393.3 | 857.3 | 6.4(5) |
| 154.0 | 436.9 | 7 (1) | 396.5 | 396.5 | 3.0(4) |
| 157 | 2046.0 | 0.3(1) | 415.1 | 1078.0 | 1.6(2) |
| 159.0 | 507.3 | 7 (1) | 416 | 649.5 | 6 (2) |
| 172.5 | 795.5 | 12 (1) | 418.0 | 795.5 | 37 (1) |
| 175.9 | 524.2 | 5.5(7) | 457.4[a] | 964.7 | 5 (1) |
| 177.2 | 1352.2 | 1.2(3) | 463.9 | 463.9 | 2.7(3) |
| 185.6 | 649.5 | 2.2(3) | 468.4 | 1117.8 | 3.4(5) |
| 192.7 | 524.2 | 2.7(4) | 483.5 | 1364.0 | 3.3(4) |
| 197.3 | 507.3 | 4 (1) | 526 | 1879 | 0.5(2) |
| 207.9 | 857.3 | 1.4(3) | 528.1 | 1835.4 | 3.5(5) |
| 210.8 | 718.1 | 5 (1) | 539.8 | 1617.8 | 1.2(2) |
| 215.3 | 309.9 | 2.3(3) | 552.3 | 1175.3 | 25 (2) |
| 232.5 | 232.5 | 21 (1) | 557.0 | 1352.5 | 18 (1) |
| 245.6 | 623.0 | 21 (2) | 583 | 1947 | 2.3(5) |
| 246.4 | 246.2 | 26 (3) | 600 | 1716.0 | 1.5(4) |
| 246.6 | 964.7 | 3 (1) | 607 | 2554 | 1.1(3) |
| 253.7 | 348.3 | 14 (2) | 651 | 2036 | 1.0(3) |
| 260.5 | 1117.8 | 0.9(3) | 658 | 2276 | 0.5(2) |
| 261.1 | 507.3 | 3.9(5) | 694 | 2046.0 | 9 (2) |
| 266.3 | 662.8 | 6 (1) | 704 | 1879 | 5 (1) |
| 274.7 | 507.3 | 4 (1) | 708 | 2426 | 0.4(2) |
| 277.8 | 524.2 | 5.4(9) | 756 | 2792 | 0.6(3) |
| 282.7 | 377.4 | 35 (2) | 826 | 2872 | 5 (1) |
| 301 | 649.5 | 4 (1) | 855 | 2734 | 2 (1) |
| 309.9 | 309.9 | 29 (2) | | | |

[a]Contaminated line.

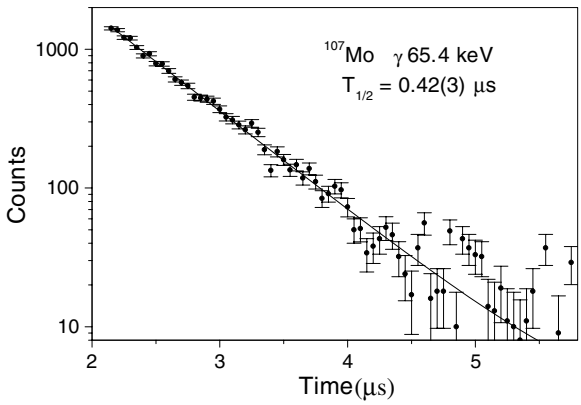


FIG. 4. Time spectrum of the 65.4-keV line in $^{107}$Mo.

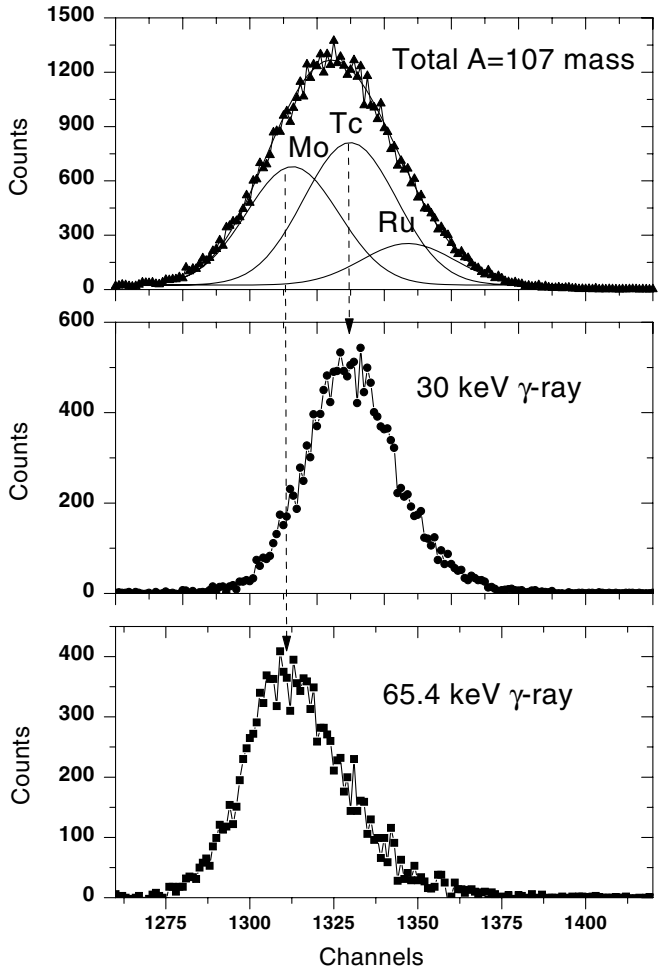


FIG. 5. Comparison of the energy lost by the FFs of mass $A = 107$ in the first region of gas of the ionization chamber, in three different cases: (a) without any conditions, (b) in coincidence with the 30 keV transition, and (c) in coincdendence with the 65.4-keV transition. In (a) the spectra of the three main isotopes contributing to the $A = 107$ mass are also reported. It is clearly evidenced in this figure that the 30- and 65.4-keV transitions belong to Tc and Mo, respectively.

peaks corresponding to conversion electrons are observed. Unseparated x-ray lines of Mo and Tc are also seen at low energies. The strong x rays of Tc are produced by another new isomeric transition of 30 keV. Its $\gamma$ line is observed in the spectrum. This new isomer will be discussed later in a forthcoming article. Other peaks in the spectrum are interpreted as due to the $K$ and $L$ conversion electrons and the $\gamma$-ray line of the 65.4-keV isomeric transition in $^{107}$Mo. For the 65.4-keV transition the comparison of the $K/L = 3.20(40)$ experimental intensity ratio with the theoretical ratios of 3.56 for $E2$, 8.60 for $E1$ and 7.88 for $M1$, respectively, shows that it is compatible with a pure $E2$ transition, only. The measured half-life of the isomeric transition allows one to compute a reduced transition probability rate $B(E2) = 180(13)\, e^2\ \mathrm{fm}^4$ or $B(E2) = 5.9(5)$ W.u.. The modest acceleration of the $B(E2)$ value strongly suggests that it is an interband transition and we propose that this isomeric transition, deexcites the $1/2^+$

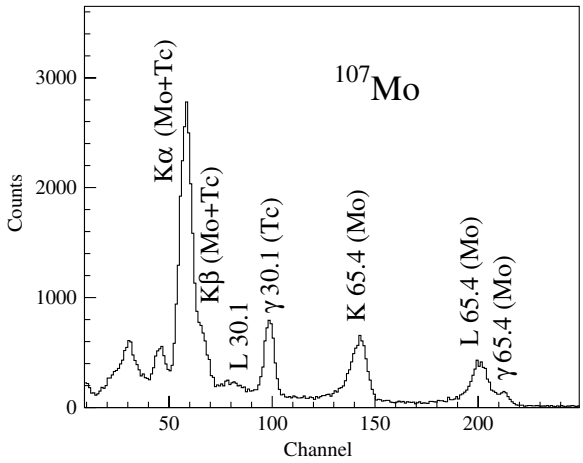


FIG. 6. Si(Li) spectrum of the $A = 107$ isomers observed in the present experiment. Narrow peaks correspond to x and $\gamma$ rays, whereas the broader peaks are due to conversion electrons.

isomeric level at 65.4 keV to the $5/2^+$ ground state of $^{107}$Mo (see below).

We stress that the new isomeric level at 65.4 keV is not the same level as the $(3/2+)$ level reported in $^{107}$Mo at 66.0 keV [7]. The half-life of the 66.0-keV level is shorter than 20 ns and the properties of the 66.0-keV transition deexciting this level indicate $M1 + E2$ character for this transition [7].

## III. QUASIPARTICLE-ROTOR-MODEL CALCULATIONS

The excited states of the bands in $^{105,107}$Mo and their $\gamma$-ray decay patterns were calculated using the code ASYRMO [19]. This code diagonalizes the particle+triaxial rotor Hamiltonian in the strong coupling basis, with the single-particle matrix elements expressed in deformed scheme, as described in Ref. [20]. Single-particle energies and various matrix elements are computed using a modified oscillator (Nilsson) potential. In the present calculation, values $\kappa = 0.068$ and $\mu = 0.35$ were taken for the strength parameters of the **ls** and $\mathbf{l^2}$ terms, for both $N = 4$ and $N = 5$ neutron shells. These values are very close to the previous $\kappa = 0.066$ and $\mu = 0.35$ values used in Ref. [21] for nuclei close to mass $A = 110$. The other parameters entering in the level calculations are pairing introduced via a standard BCS calculation, the deformation parameters $\epsilon_2$ and $\gamma$ of the single-particle potential in the intrinsic system and the inertia parameter, $a$, of the bands. Agreement with theory can be improved by introducing an *ad hoc* "Coriolis attenuation" parameter, $\xi$. An effective value $\xi = 0.7$ is common in these calculations. Finally, the number of variable parameters was minimized by imposing that all bands of the same nucleus have the same parameter values.

### A. $^{105}$Mo nucleus

Figure 7 gives the results of the calculation for the lowest four bands in $^{105}$Mo. Assuming that this nucleus is axially symmetric the best fit to the experimental data is obtained for the deformation $\epsilon_2 = 0.32$ $\beta_2 = 0.39$, the inertia parameter

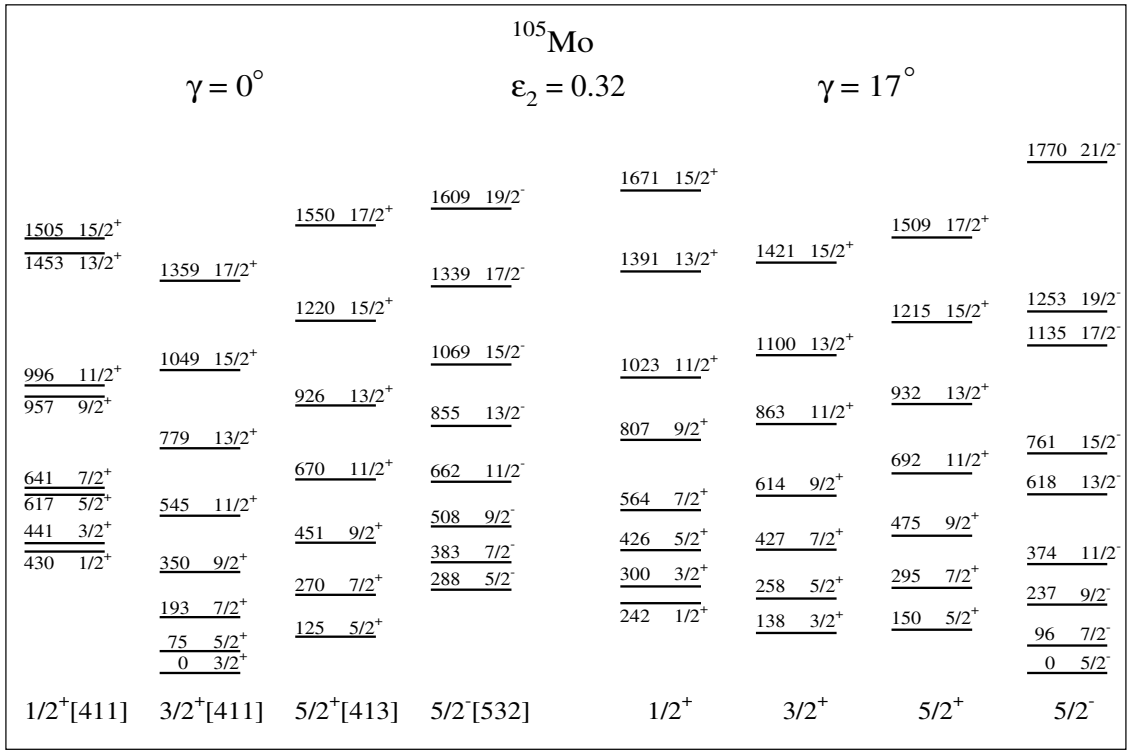


FIG. 7. Calculated levels for the four bands in $^{105}$Mo performed for $\gamma$ deformations 0° and 17°, respectively. It is worth noting that the staggering in the $1/2^+$ and $5/2^-$ differs strongly for these two deformations.

$a = 23.3$ keV, and the Coriolis attenuation parameter $\xi = 0.70$. This result suggests that the four experimentally observed bands (1)–(4) occupy the 5/2[532], 5/2[413], 3/2[411], and 1/2[411] Nilsson states, respectively. The first configuration originates mainly from the $h_{11/2}$ unique parity state and its band is strongly affected by the Coriolis coupling. The comparison between experiment and theory for an axially symmetric shape shows important discrepancies. The theory predicts the 3/2[411] ground-state level, whereas the $5/2^-$ level is observed experimentally. Moreover, the signature splittings of 1/2[411] and 5/2[532] bands are not correctly reproduced by the model. To try to cure the observed inconsistencies, we have assumed that $^{105}$Mo has a well-defined asymmetric equilibrium shape and analyzed the effect of the triaxial deformation on the staggering of the $1/2^+$ band. In this new calculation we have kept unchanged the other parameters values $\epsilon_2 = 0.32$, $a = 23.3$ keV, and $\xi = 0.70$. In the triaxial calculation the rotational bands are labeled by the spin of the their band heads. Figure 8 shows that the signature splitting changes as a function of the $\gamma$ deformation and that the experimental levels of the $1/2^+$ band are well reproduced at the deformation $\gamma = 17^\circ$. Moreover, Fig. 7 shows that all four bands are much better reproduced by the model at this $\gamma$ deformation. The $5/2^-$ level is now the ground state of the $^{105}$Mo nucleus, as seen in the experiment. There is still some discrepancy because the $5/2^-$ level is about 120 keV too high in energy. We note that the $\kappa$ and $\mu$ parameters are chosen to be identical for the $N = 4$ and $N = 5$ shells in this calculation, which could be the origin of the discrepancy. Finally, Fig. 9 shows that the staggering in $1/2^+$ and the $5/2^-$ bands is much better reproduced by assuming $\gamma$ deformation of 17°. The computation also shows that levels of each rotational band have a dominant $K$ value in the asymmetric model, though the $K$ mixing increases with spin.

To complete the theoretical analysis of the energy levels, the $\gamma$-decay patterns of both intraband and interband transitions were also computed. For this purpose, only $M1$ and $E2$ matrix elements were computed at $\gamma = 17^\circ$, and a collective $g$-factor value of the core, $g_R = 0.2$, and an effective value of the free neutron $g$ factor, $g_s^{\text{eff}} = 0.7 \times g_s^{\text{free}}$, were extracted from

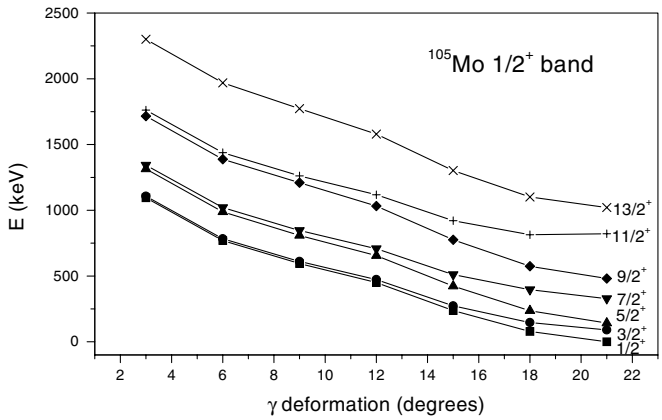


FIG. 8. Variation of the theoretical energy levels of the $1/2^+$ band in $^{105}$Mo as function of $\gamma$ deformation.

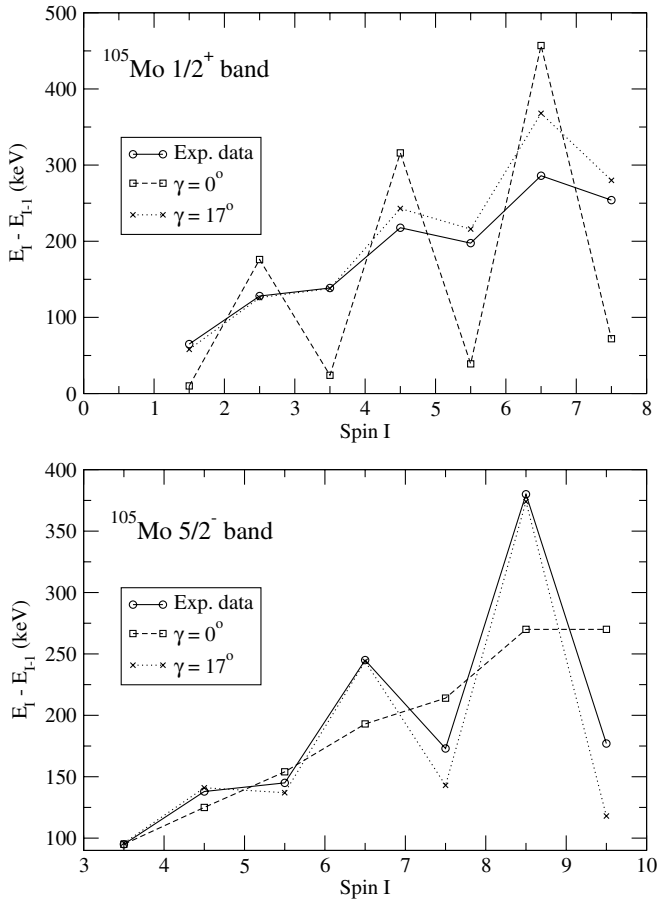


FIG. 9. Comparison of the experimental staggering observed in the $1/2^+$ and $5/2^-$ bands of $^{105}$Mo with theory for $\gamma$ deformations 0° and 17°, respectively.

TABLE II. Comparison of the experimental and theoretical $\gamma$-branching ratios and half-lives of low-lying levels in $^{105}$Mo. In columns 1 and 2 experimental level- and $\gamma$-ray energies are reported.

| $E_{\text{level}}$ (keV) | $E_\gamma$ (keV) | $I_\gamma$ (rel.) Theo. | $I_\gamma$ (rel.) Exp. | $T_{1/2}$ (ps) Theo. | $T_{1/2}$ (ps) Exp. [7] |
|---|---|---|---|---|---|
| Positive-parity states | | | | | |
| 331.5 | | | | 1031 | |
| 396.5 | 65 | 3 | | | |
| | 149.8 | 100 | 100 | | |
| 463.9 | 115.5 | 100 | 100 | | |
| | 154 | 32 | 117(26) | | |
| | 217.5 | 14 | | | |
| 507.3 | 159 | 100 | 100 | <77 | 83(50) |
| | 197.3 | 25 | 57(13) | | |
| | 261 | 56 | 56(16) | | |
| 524.2 | 127.8 | 56 | 42(10) | 170 | 101(47) |
| | 175.9 | 68 | 102(21) | | |
| | 192.7 | 67 | 49(11) | | |
| | 277.8 | 100 | 100 | | |
| 649.5 | 185.6 | 36 | 44(11) | | |
| | 301 | 12 | 80(26) | | |
| | 339.6 | 100 | 100 | | |
| 662.8 | 266.3 | 100 | 100 | | |
| | 314.5 | 214 | 35(8) | | |
| Negative-parity states | | | | | |
| 94.7 | 94.7 | 100 | 100 | 800 | 480(40) |
| 232.5 | 232.5 | 50 | 28(2) | 167 | 111(10) |
| | 137.8 | 100 | 100 | | |
| 377.4 | 144.8 | 100 | 100 | 64 | |
| | 282.7 | 132 | 45(3) | | |
| 623 | 245.6 | 43 | 60(7) | 14 | |
| | 390.5 | 100 | 100 | | |

the best fit to the experimental data. For the comparison of the theoretical branching ratios or half-lives with experiment, the experimental transition energies were used in place of the theoretical ones and conversion coefficients were taken into account. Table II shows that the $\gamma$-branching ratios are generally correctly reproduced by the model. The computed half-lives are generally overestimated by about 60% in comparison with the measurements of Liang *et al.* [9], which are shown in Table II. In contrast, the theoretical value of $T_{1/2} = 803$ ps for the 94.7-keV transition is in much better agreement with the previous values of 800 [22] and 1110 ps [23], respectively, than with the 480-ps value found by Liang [9].

Very recently the magnetic moments of the low-lying excited states in the $5/2^-$ band of $^{105}$Mo were measured for the first time [6]. The authors compared these new experimental data and the energy levels of the band with the predictions of a particle-rotor model, to investigate the triaxiality in this nucleus. They have found that the signature splitting of the $5/2^-$ band is correctly reproduced assuming a triaxial deformation ($\beta_2 = 0.36, \gamma = 15°$) for $^{105}$Mo [6]. This result is close to the deformation we have obtained from a fit to the four bands in $^{105}$Mo ($\beta_2 = 0.38, \gamma = 17°$). Another deformation ($\beta_2 = 0.36, \gamma = 7°$) was also used in Ref. [6] to better reproduce the experimental magnetic moments of the first $7/2^-$ and $9/2^-$ states in $^{105}$Mo. However, this smaller triaxial value is unable to correctly reproduce the signature splitting of the $5/2^-$ band (1), as well as the staggering and the energy position of the $1/2^+$ band (4), and is very likely not realistic. In Table III, the experimental magnetic moments are compared with the predictions of Ref. [6] and our calculations. Although our predictions are slightly closer to the experimental data than the ones of Ref. [6], in both cases theory overestimates the experimental values.

One of the parameters used in the analysis of magnetic moments is the collective giromagnetic ratio, $g_R$. This quantity is difficult to extract from experimental data and is strongly model dependent. Nevertheless, the $g_R = 0.2$ value found in

TABLE III. Comparison of the experimental magnetic moments in the $5/2^-$ band of $^{105}$Mo with our theoretical predictions and the ones of Ref. [6].

| $I^\pi$ | Exp. $\mu_N$ | $\mu_{\text{Theo.}}$ $\mu_N$ | $\mu_{\text{Theo.}}$ (Ref. [6]) $\mu_N$ |
|---|---|---|---|
| $7/2^-$ | −0.224(28) | −0.558 | −0.615 |
| $9/2^-$ | −0.12(16) | −0.378 | −0.489 |

this work, from the calculations of the $M1$ matrix elements and the comparison with the experimental data, is comparable to the values $g_R = 0.13(2)$ and $g_R = 0.11(4)$ reported in Table IV of Ref. [6] and the $g_R = 0.15(2)$ value used by the same authors in their particle-rotor calculations. Consequently, one may conclude from these different analysis that a $g_R = 0.15$–$0.20$ value is a good estimate of this quantity.

### B. $^{107}$Mo nucleus

An analogous theoretical analysis was performed for $^{107}$Mo. In this case only three bands were previously identified [7]. We propose that the new $1/2^+$ microsecond isomeric level is the head of a new band, analogous to the $1/2^+$ band observed in $^{105}$Mo. For the $^{107}$Mo nucleus, the best fit to the experimental data is obtained for deformation parameters $\epsilon_2 = 0.32$ and $\gamma = 16.5^\circ$, an inertia parameter $a = 25$ keV, and the Coriolis attenuation parameter $\xi = 0.70$. The experimental positive-parity levels are well reproduced by the model, as shown in Fig. 10. The three bands are analogous to the three positive-parity bands observed in $^{105}$Mo, though the relative position of their band heads is different than in $^{105}$Mo. The main consequence of these differences is that the $1/2^+$ state in $^{107}$Mo has lower energy than in $^{105}$Mo and becomes an isomer in $^{107}$Mo. Similarly, as discussed in the case of $^{105}$Mo, there is a discrepancy for the $7/2^-$ state, which is calculated 295 keV too low in energy in $^{107}$Mo. In this band, a $5/2^-$ state is also predicted by theory 80 keV lower than the $7/2^-$ state. Although it was not observed experimentally in previous works [4,7], it is not possible to fully discard the presence of the $5/2^-$ level in $^{107}$Mo.

Half-lives and branching ratios were also computed and are compared with experimental data in Table IV. The $1/2^+$, $T_{1/2} = 420(30)$-ns isomer at 65.4-keV decays by an $E2$ transition to the $5/2^+$ ground state. In spite of the strong configuration mixing present in these two levels, the theoretical half-life, $T_{1/2} = 200$ ns, is not far from the experimental value. The theoretical branching ratios generally agree with theory, but it is worth noting that the relatively strong feeding of the $5/2^+$ ground state through the 165.4-keV transition is not reproduced by theory. No good explanation was found for this effect and it is the main discrepancy, concerning the $\gamma$-decay pattern observed in this nucleus.

TABLE IV. Comparison of the experimental and theoretical $\gamma$-branching ratios and half-life of the isomeric transition in $^{107}$Mo. In columns 1 and 2 experimental level- and $\gamma$-ray energies are reported.

| $E_{\text{level}}$ (keV) | $E_\gamma$ (Rel.) (keV) | $I_\gamma$ (Rel.) Theo. | $I_\gamma$ Exp. | $T_{1/2}$ (ps) Theo. | $T_{1/2}$ (ps) Exp. |
|---|---|---|---|---|---|
| Positive-parity states | | | | | |
| 66 | 66 | 100 | 100 | 200 | 420 |
| 165.4 | 99.4 | 100 | 100 | | |
| | 165.4 | 4 | 163(28) | | |
| 319.7 | 154.3 | 100 | 100 | | |
| | 253.7 | 50 | 113(15) | | |
| 341.0 | 188.9 | 31 | 28(4) | | |
| | 341.0 | 100 | 100 | | |
| 491.7 | 171.9 | 38 | 31(6) | | |
| | 226.3 | 100 | 100 | | |
| Negative-parity states | | | | | |
| 581.9 | 123.4 | 100 | 100 | | |
| | 233.6 | 100 | 49(5) | | |
| 838.3 | 256.1 | 45 | 79(13) | | |
| | 379.5 | 100 | 100 | | |

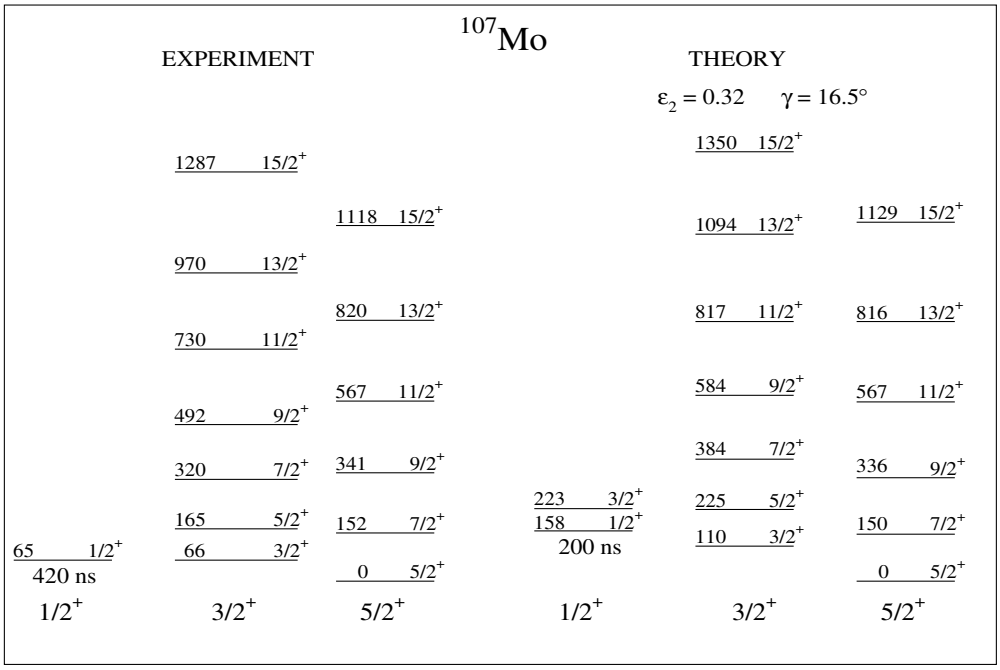


FIG. 10. Comparison of the experimental levels of the three positive-parity bands in $^{107}$Mo with theory.

## IV. COMPARISON BETWEEN ODD AND EVEN-EVEN Mo NUCLEI

In the previous section it was shown that a satisfactory fit to the experimental data has been obtained using the simple particle-rotor calculations for both $^{105}$Mo and $^{107}$Mo and assuming that these nuclei are asymmetric rotors with remarkably similar deformations, $\epsilon_2 = 0.32$ and $\gamma \approx 17^\circ$. It is worth noting that four bands of the same origin observed in these two nuclei are well reproduced by these parameters. The main deviation between the experiment and the theory concerns the position of the the band-head energy of the negative-parity band, originating from the $h_{11/2}$ orbital. As discussed above, the origin of this discrepancy could be either due to the parameters of the Nilsson model being not correctly adjusted for the $N = 5$ shell or due to a possible differences of deformations in positive- and negative-parity states. The last point is, however, less probable because the signature splitting of these two $5/2^-$ bands is well reproduced by the model.

It is instructive to compare the deformation parameters found in these odd-$A$ nuclei with the corresponding parameters in the even-even $^{104}$Mo-$^{108}$Mo isotopes. If one supposes that these even Mo isotopes have triaxial minima at low spins, it is possible to extract the nonaxiality $\gamma$ parameter from the experimental data. For this purpose, we have used the Davydov and Filippov theory [24], which supposes a rigid triaxiality, but allows the extraction of nearly identical $\gamma$ values for $\gamma$-soft or $\gamma$-rigid potentials [25,26]. In this model, the $\gamma$ parameter can be obtained from the ratio of energies of the second and first excited $2^+$ states and from the branching ratio $R_b = B(E2; 2_2 \rightarrow 2_1)/B(E2; 2_2 \rightarrow 0_1)$. In the latter case, it was assumed that the $M1$ fraction of the $2_2^+ \rightarrow 2_1^+$ transition is small, as predicted by the model, and it is not taken into account in the calculation for half-life computations. The values obtained by the two methods and presented in Table V are comparable. The mean value for $^{104}$Mo and $^{106}$Mo, $\gamma = 19.1^\circ$, is only slightly larger than the value for $^{105}$Mo, $\gamma = 17^\circ$. Similarly, the mean value for $^{106}$Mo and $^{108}$Mo, $\gamma = 20.5^\circ$ is also close to the value for $^{107}$Mo, $\gamma = 16.5^\circ$. The quadrupole deformations of the even Mo isotopes can be obtained from the experimental $B(E2; 2_1 \rightarrow 0_1)$ values [27,28] and the previously obtained $\gamma$ deformations, using Eq. (4) of Ref. [26]. The mean value for $^{104,106,108}$Mo ($\epsilon_2 = 0.31$) is very close to the value found for the $^{105-107}$Mo ($\epsilon_2 = 0.32$). In conclusion, at low spins the considered even and odd Mo isotopes, in the neutron range $N = 62$–$66$, have comparable triaxial minima ($\epsilon_2 \approx 0.31$–$0.32$, $\gamma \approx 17^\circ$–$21^\circ$), if a nonzero $\gamma$ deformation for the even Mo is supposed. Moreover, a comparable triaxial deformation ($\epsilon_2 \approx 0.32$, $\gamma \approx 22^\circ$) was also reported for $^{107}$Tc, with $N = 64$ neutrons [29]. All these data strongly suggest that the cores have similar shapes in the heavy even-even and odd-neutron Mo nuclei, as well as in the odd-proton Tc nuclei, and that the odd-$A$ nuclei are not strongly affected by the unpaired particle. The hypothesis of a stable triaxial deformation at low spins in the $g$ band of $^{104,106,108}$Mo agrees with the calculations of Skalski *et al.*, predicting ($\gamma = 17^\circ, 17^\circ, 21^\circ$) at spins $I = 0$–$6$ for all three isotopes, respectively (see Fig. 15 of Ref. [5]), though the predicted quadrupole deformation $\beta_2 \approx 0.31$, ($\epsilon_2 \approx 0.27$) is subtantially smaller than the corresponding value $\beta_2 \approx 0.38$ reported in Table V.

From a comparison of the experimental crossing frequency of the $g$ and $S$ band in $^{104}$Mo with a cranked shell-model calculation, Hua *et al.* [4] have deduced a deformation ($\beta_2 \approx 0.33, \gamma \approx 19^\circ$). This value agrees with the predictions of Skalsky *et al.* ($\beta_2 \approx 0.30, \gamma \approx 21^\circ$) for the spin region $I = 14$–$16$. The comparison of the deformation reported in Table V ($\beta_2 \approx 0.38$) with the results of Hua *et al.* indicates a decrease of the quadrupole deformation between the low-spin and the back-bending region. The calculations of Skalski *et al.* predicts also a rapid change of the shape of Mo isotopes from $^{104}$Mo to $^{108}$Mo. For instance, a deformation ($\beta_2 \approx 0.28, \gamma \approx 30^\circ$) is expected for $^{108}$Mo at $I \approx 14$. Unfortunately, the comparison with theory is not possible because experimental triaxial-deformation values for $^{106}$Mo and $^{108}$Mo were not reported in the Hua *et al.* article, although the crossing frequencies were measured for these two nuclei.

TABLE V. $\gamma$ deformation values for even-even Mo obtained from values of $R_a = E(2_2)/E(2_1)$ and $R_b = B(E2; 2_2 \rightarrow 2_1)/B(E2; 2_2 \rightarrow 0_1)$ (see text). The mean value is also shown for each nucleus. The parameters of quadrupole deformation, $\epsilon_2$ and $\beta_2$, are deduced from the $\gamma$ values and the experimental $B(E2; 2_1 \rightarrow 0_1)$ values [27,28].

| $\gamma$ deformation | $^{104}$Mo | $^{106}$Mo | $^{108}$Mo |
|---|---|---|---|
| $\gamma_a$ | 18.8° | 19° | 22.1° |
| $\gamma_b$ | 20.4° | 18.2° | 23.7° |
| Mean value | 19.6° | 18.6° | 22.4° |
| Deformation $\epsilon_2$ | 0.308(5) | 0.310(7) | 0.310(32) |
| Deformation $\beta_2$ | 0.375(8) | 0.378(9) | 0.378(38) |

## V. CONCLUSIONS

In conclusion, the amount of information collected in $^{105}$Mo from prompt $\gamma$ rays emitted from FFs of $^{248}$Cm has allowed a complex level scheme to be built, comprising four well-developed rotational bands. The evidence of a new low-lying $\mu$s isomer in $^{107}$Mo, obtained from thermal-neutron induced fission of $^{241}$Pu, suggests that it is the band head of the $1/2^+$ rotational band also observed in $^{105}$Mo. Consequently, three bands previously reported in [7] and the ground state of a fourth band are now experimentally known in $^{107}$Mo. This wealth of information makes a comparison in the frame of rotational models meaningful. A satisfactory fit to the experimental data has been obtained for both $^{105}$Mo and $^{107}$Mo in a simple particle-rotor calculations, assuming that these nuclei are asymmetric rotors. The parameters of the model are very similar for both nuclei and indicate values of deformation parameters $\epsilon_2 = 0.32$ and $\gamma \approx 17^\circ$. It is important to note that in both nuclei all four bands are well reproduced using the same $\gamma$ parameters. Moreover, in the neutron range $N = 62$–$66$, the $\gamma$ deformation of the odd Mo are very close to the values of the even-even Mo, suggesting

that all these nuclei have comparable core deformations, $\epsilon_2 = 0.31$–$0.32$, $\gamma = 17^\circ$–$22^\circ$.

## ACKNOWLEDGMENTS

This work was supported by the French-Polish IN2P3-KBN collaboration no. 01-100 and by the U.S. Department of Energy under contract W-31-109-ENG-38. The authors are indebted for the use of $^{248}$Cm to the Office of Basic Energy Sciences, U.S. Department of Energy, through the transplutonium element production facilities at the Oak Ridge National Laboratory. I. Deloncle and M.-G. Porquet are gratefully acknowledged for helpful discussion.

[1] W. Urban, J. A. Pinston, J. Genevey, T. Rząca-Urban, A. Złomaniec, G. Simpson, J. L. Durell, W. R. Phillips, A. G. Smith, B. J. Varley, I. Ahmad, and N. Schulz, Eur. Phys. J. A **22**, 241 (2004).

[2] A. G. Smith, J. L. Durell, W. R. Phillips, M. A. Jones, M. Leddy, W. Urban, B. J. Varley, I. Ahmad, L. R. Morss, M. Bentaleb, A. Guessous, E. Lubkiewicz, N. Schulz, and R. Wyss, Phys. Rev. Lett. **77**, 1711 (1996).

[3] A. Guessous, N. Schulz, M. Bentaleb, E. Lubkiewicz, J. L. Durell, C. J. Pearson, W. R. Phillips, J. A. Shannon, W. Urban, B. J. Varley, I. Ahmad, C. J. Lister, L. R. Morss, K. L. Nash, C. W. Williams, and S. Khazrouni, Phys. Rev. C **53**, 1191 (1996).

[4] H. Hua, C. Y. Wu, D. Cline, A. B. Hayes, R. Teng, R. M. Clark, P. Fallon, A. Goergen, A. O. Macchiavelli, and K. Vetter, Phys. Rev. C **69**, 014317 (2004).

[5] J. Skalski, S. Mizutory, and W. Nazarewicz, Nucl. Phys. **A617**, 282 (1997).

[6] R. Orlandi, A. G. Smith, D. Patel, G. S. Simpson, R. M. Wall, J. F. Smith, O. J. Onakanmi, I. Ahmad, J. P. Greene, M. P. Carpenter, T. Lauritsen, C. J. Lister, R. V. F. Janssens, F. G. Kondev, D. Seweryniak, B. J. P. Gall, O. Dorveaux, and A. E. Stuchbery, Phys. Rev. C **73**, 054310 (2006).

[7] W. Urban, T. Rząca-Urban, J. A. Pinston, J. L. Durell, W. R. Phillips, A. G. Smith, B. J. Varley, I. Ahmad, and N. Schulz, Phys. Rev. C **72**, 027302 (2005).

[8] K. Shizuma, H. Ahrens, J. P. Boucquet, B. D. Kern, H. Lawin, R. A. Meyer, K. Sistemich, G. Tittel, and N. Trautmann, Z. Phys. A **351**, 13 (1995).

[9] M. Liang, H. Ohm, B. De Sutter-Pomme, and K. Sistemich, Z. Phys. A **351**, 13 (1995).

[10] G. Lhersonneau, P. Dendooven, A. Honkanen, M. Huhta, M. Oinonen, H. Penttila, J. Aisto, J Kurpeta, J. R. Persson, and A. Popov, Phys. Rev. C **54**, 1592 (1996).

[11] M. C. A. Hotchkis, J. L. Durell, J. B. Fitzgerald, A. S. Mowbray, W. R. Phillips, I. Ahmad, M. P. Carpenter, R. V. F. Janssens, T. L. Khoo, E. F. Moore, L. R. Morss, Ph. Benet, and D. Ye, Nucl. Phys. **A530**, 111 (1991).

[12] J. K. Hwang, A. V. Ramayya, J. H. Hamilton, J. Kormicki *et al.*, J. Phys. G: Nucl. Part. Phys. **24**, L9 (1998).

[13] T. Rząca-Urban, W. R. Phillips, J. L. Durell, W. Urban, B. J. Varley, C. J. Pearson, J. A. Shannon, I. Ahmad, C. J. Lister, L. R. Morss, K. L. Nash, C. W. Williams, M. Bentaleb, E. Lubkiewicz, and N. Schulz, Phys. Lett. **B348**, 336 (1995).

[14] W. Urban, J. L. Durell, W. R. Phillips, A. G. Smith, M. A. Jones, I. Ahmad, A. R. Barnet, S. J. Dorning, M. J. Leddy, E. Lubkiewicz, L. R. Morss, T. Rząca-Urban, R. A. Sareen, N. Schulz, and B. J. Varley, Z. Phys. A **358**, 145 (1997).

[15] M. A. Jones, W. Urban, and W. R. Phillips, Rev. Sci. Instr. **69**, 4120 (1998).

[16] J. Genevey, F. Ibrahim, J. A. Pinston, H. Faust, T. Friedrichs, M. Gross, and S. Oberstedt, Phys. Rev. C **59**, 82 (1999).

[17] J. A. Pinston and J. Genevey, J. Phys. G: Nucl. Part. Phys. **30**, R57 (2004).

[18] J. Genevey, R. Gugliemmini, R. Orlandi, J. A. Pinston, A. Scherillo, G. Simpson, I. Tsekhanovich, N. Warr, and J. Jolie, Phys. Rev. C **73**, 037308 (2006).

[19] P. Semmes and I. Ragnarsson, *The Particle plus Triaxial Model: A User's Guide*, distributed at the Hands-on Nuclear Physics Workshop, Oak Ridge, 5–16 August 1991 (unpublished).

[20] S. E. Larsson, G. Leander, and I. Ragnarsson, Nucl. Phys. **A307**, 189 (1978).

[21] R. A. Meyer, E. Monnand, J. A. Pinston, F. Schussler, I. Ragnarsson, B. Pfeiffer, H. Lawin, G. Lhersonneau, T. Seo, and K. Sistemich, Nucl. Phys. **A439**, 510 (1985).

[22] H. A. Selic, E. Cheifetz, and J. B. Wilhelmy, Annual Report, KFA Julich, Jul-Spez-99, 1981.

[23] R. L. Watson, J. B. Wilhelmy, R. C. Jared, C. Rugge, H. R. Bowmann, S. G. Thompson, and J. O. Rasmussen, and K. Sistemich, Nucl. Phys. **A141**, 449 (1970).

[24] A. S. Davydov, and G. F. Filippov, Nucl. Phys. **A8**, 237 (1958).

[25] N. V. Zamfir and R. F. Casten, Phys. Lett. **B260**, 265 (1991).

[26] L. Esser, U. Neuneyer, R. F. Casten, and P. von Brentano, Phys. Rev. C **55**, 206 (1997).

[27] C. Hutter *et al.*, Phys. Rev. C **67**, 054315 (2003).

[28] S. Raman, C. H. Malarkey, W. T. Milner, C. W. Nestor Jr., and P. H. Stelson, At. Data Nucl. Data Tables **36**, 1 (1987).

[29] Y. X. Luo *et al.*, Phys. Rev. C **70**, 044310 (2004).